

Computational Modeling of the Triplet Metal-to-Ligand Charge-Transfer Excited-State Structures of Mono-Bipyridine–Ruthenium(II) Complexes and Comparisons to their 77 K Emission Band Shapes

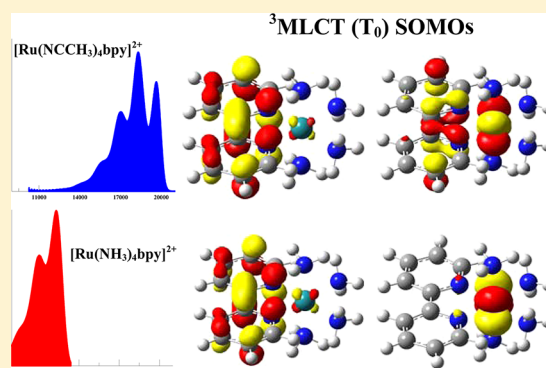
Richard L. Lord,[†] Marco M. Allard,[†] Ryan A. Thomas,[†] Onduro S. Odongo,[†] H. Bernhard Schlegel,^{*,†} Yuan-Jang Chen,[‡] and John F. Endicott^{*,†}

[†]Department of Chemistry, Wayne State University, Detroit, Michigan 48202, United States

[‡]Department of Chemistry, Fu Jen Catholic University, New Taipei City 24205, Taiwan, Republic of China

Supporting Information

ABSTRACT: A computational approach for calculating the distortions in the lowest energy triplet metal to ligand charge-transfer (³MLCT = T₀) excited states of ruthenium(II)–bipyridine (Ru–bpy) complexes is used to account for the patterns of large variations in vibronic sideband amplitudes found in the experimental 77 K emission spectra of complexes with different ancillary ligands (L). Monobipyridine, [Ru(L)₄bpy]^{m+} complexes are targeted to simplify analysis. The range of known emission energies for this class of complexes is expanded with the 77 K spectra of the complexes with (L)₄ = bis-acetonacetonate (emission onset at about 12 000 cm⁻¹) and 1,4,8,11-tetrathiacyclotetradecane and tetrakis-acetonitrile (emission onsets at about 21 000 cm⁻¹); no vibronic sidebands are resolved for the first of these, but they dominate the spectra of the last two. The computational modeling of excited-state distortions within a Franck–Condon approximation indicates that there are more than a dozen important distortion modes including metal–ligand modes (low frequency; *lf*) as well as predominately bpy modes (medium frequency; *mf*), and it simulates the observed 77 K emission spectral band shapes of selected complexes very well. This modeling shows that the relative importance of the *mf* modes increases very strongly as the T₀ energy increases. Furthermore, the calculated metal-centered SOMOs show a substantial bpy– π -orbital contribution for the complexes with the highest energy T₀. These features are attributed to configurational mixing between the diabatic MLCT and the bpy ³ $\pi\pi^*$ excited states at the highest T₀ energies.



INTRODUCTION

The spectroscopic and oxidation/reduction properties of the lowest energy metal-to-ligand charge-transfer (³MLCT) excited states of transition metal polypyridine complexes have been examined extensively,^{1–3} and they have been used or proposed for use as high-energy electron donors (D) or acceptors (A) in a wide range of applications.^{4–15} The rates of the implicated electron-transfer reactions are functions of the energies, electronic configurations, and nuclear structures of the excited states.^{7,16,17} Electron transfer to an external acceptor occurs in competition with processes that quench the excited states (see Figure 1). The rates of these competitive processes generally depend differently on the excited-state energies and nuclear coordinates, and the processes usually have different purely electronic constraints (such as donor–acceptor orbital spatial overlap).^{7,18–20} As a consequence, design of systems that can achieve efficient and selective electron-transfer reactivity that is required for many applications necessitates an understanding of variations of the molecular and electronic structures of the excited states as well as their energies when their coordination

environments are changed. Since the excited-state lifetimes are short, this information has been difficult to obtain.

In the simplest limit MLCT excited states correspond to transfer of an electron from Ru^{II} to a bpy ligand (see Figure 1) accompanied by changes of the metal–ligand and bpy bond lengths and angles. These changes in the nuclear coordinates give rise to the vibronic sidebands found in the emission spectra, and the amplitudes of the sidebands that are attributable to the bpy ligand, $A_{v_m(\text{bpy})}$, are correlated with the net differences in electronic charge on the ligand in the ground and excited states²¹ and result from the convoluted contributions from many distortion modes.^{22–28} We previously found that $A_{v_m(\text{bpy})}$ increases systematically with the energy of the ³MLCT excited state for simple Ru/bpy complexes.^{25,27,28} For example, the highest energy emission sideband envelopes of the [Ru(acac)(bpy)₂]⁺ and [Ru(CH₃CN)₂(bpy)₂]²⁺ complexes at 77 K have about 75% and 100% of the amplitudes of

Received: May 7, 2012

Published: January 23, 2013

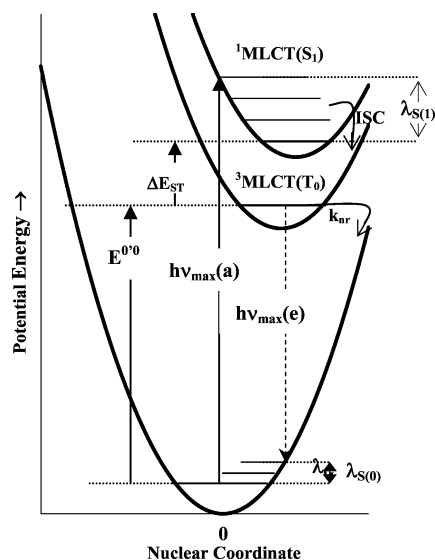


Figure 1. Qualitative potential energy diagram illustrating the terms and processes considered for a three state system with $^1\text{MLCT}$ and $^3\text{MLCT}$ excited states. Since this figure represents an idealized (diabatic) limit, $\Delta E_{\text{ST}} = 2K_{\text{exch}}$ where K_{exch} is the exchange energy; in actual spectra ΔE_{ST} is more complicated.

their respective emission maxima (at 13 800 and 18 400 cm^{-1}).²⁷ In this study we examined experimentally and computationally the simpler $[\text{Ru}(\text{L}_4)\text{bpy}]^{m+}$ complexes over an expanded range of emission energies and band shapes and find that the general pattern of increasing sideband amplitudes with increasing energy continues through the extended energy range. If the *mf* vibronic sideband amplitudes were proportional to the amount of charge transferred to bpy in the $^3\text{MLCT}$ excited state, then the charge transferred must be greater for high- than for low-energy excited states. In one approach (A), models for $^3\text{MLCT}$ excited-state structures have been based, at least implicitly, on transfer of one electron from Ru^{II} to bpy accompanied by distortions in a single average low-frequency (*lf*; $h\nu_{\text{vib}} < 1000 \text{ cm}^{-1}$) and a single average medium-frequency (*mf*; $1000 < h\nu_{\text{vib}}/\text{cm}^{-1} \leq 1600$) vibrational mode and several parameters to adjust for spectral fits.^{29–31} Such models cannot properly represent excited-state molecular structures of systems in which the distortion is spread over many different vibrational modes, and they necessarily overestimate the excited-state electron-transfer reorganizational energies. A second approach (B) has dealt with the multimode excited-state distortions by modeling vibronic sideband shapes using reported resonance-Raman (rR) parameters.^{22–24} This approach demonstrated that the contributions of *mf* modes in Ru–bpy complexes decreases with excited-state energy; however, it also depends on adjustable parameters and generally requires additional vibronic contributions for good fits of 77 K spectra.^{25,27,28} Neither of these approaches, A or B, provides insight into the origins of the variations of vibronic sideband amplitudes with excited-state energy.

Ideally one should investigate the origin of emission spectral band shape variations without the extraneous assumptions in models A and B. Density functional theory (DFT) approaches this ideal because it is minimally parametrized based on systems different from those in this report.^{32–35} Several recent studies have used computational approaches to model the lowest energy triplet metal-centered and charge-transfer excited states of Ru complexes.^{36–50} We employ a recent approach by Barone

et al. that allows for efficient simulation of vibronically resolved spectra within the Franck–Condon approximation.^{51–53} This is the first time this approach has been used to study Ru–bpy charge-transfer excited states. Our results for distortions of the $[\text{Ru}(\text{L}_4)\text{bpy}]^{m+}$ $^3\text{MLCT}$ excited states demonstrate that they (a) differ over the $^3\text{MLCT}$ energy range due to the complementary contributions of excited/excited-state mixing and ground/excited-state mixing and (b) are large in several modes in both the *lf* and the *mf* regimes so that harmonics and combination bands make appreciable contributions to emission band shapes.

EXPERIMENTAL SECTION

The following commercial chemicals were used with no further purification: DMSO; 1,4,8,11-tetrathiaclotetradecane ($[\text{14}] \text{aneS}_4$); 2,2'-bipyridine; acetylacetonate (acac); CH_3CN ; NH_4PF_6 ; NaCl. Syntheses of the $[\text{Ru}(\text{L}_4)\text{bpy}]^{m+}$ complexes with $(\text{L})_4 = (\text{acac})_2$,^{54,55} $(\text{CH}_3\text{CN})_4$,^{54,56} and $[\text{14}] \text{aneS}_4$ ⁵⁷ have been reported previously.

Spectral determinations in solutions of $[\text{Ru}(\text{CH}_3\text{CN})_4\text{bpy}]^{2+}$ and $[\text{Ru}([\text{14}] \text{aneS}_4)\text{bpy}]^{2+}$ exhibited impurity emissions unless great care was taken, and scattered light was a problem with the latter. The reported syntheses frequently resulted in complexes with small amounts of impurities that contributed to the 77 K emission especially for excitation energies that were well removed from the absorption maxima. We used several variations on the synthesis of each complex, and several emission spectra were determined for each preparation. The principle impurity found was $[\text{Ru}(\text{bpy})_3]^{2+}$, most likely produced in a refluxing step. To minimize this impurity we modified the literature syntheses^{57,58} with a slow, dilute addition of bipyridine in the dark and in an Ar atmosphere and a longer reflux time at 40 °C. The modifications greatly reduced the impurity emissions. The impurity emissions complicated determination of the lowest energy spectral amplitudes but did not significantly alter the ratios of the two highest energy emission components. Cutoff filters were used to remove most of the scattered excitation light. However, the very weak emission of the $[\text{Ru}([\text{14}] \text{aneS}_4)\text{bpy}]^{2+}$ complex necessitated the use of relatively large input slit widths, so impurity emission and second-order scattered excitation light (detected in spectra at about 810 nm for 405 nm excitation) were significant problems in the acquisition of good quality spectra.

Samples were prepared anaerobically (Ar purge) in dimmed light. Solutions for emission spectra were frozen as soon as the complex salt dissolved in butyronitrile. See Supporting Information Figure S1 for further details and ^1H NMR spectra of the $[\text{Ru}(\text{CH}_3\text{CN})_4\text{bpy}]^{2+}$ and $[\text{Ru}([\text{14}] \text{aneS}_4)\text{bpy}]^{2+}$ complexes.⁵⁹

Instrumentation. $[\text{Ru}(\text{acac})_2\text{bpy}]$ emission spectra were collected using (a) the PI InGaAs detector and samples cooled to 77 K as described previously^{27,28} and (b) the ANDOR spectrometer system with the NIR iDUS camera. Emission spectra were indistinguishable at the maximum and higher energies but broader on the low-energy side in the earlier determination. Emission spectra of the complexes reported here for the first time were collected using an ANDOR Shamrock 500 spectrometer with dual exit ports and equipped with three gratings: 150 L/mm, 800 nm blaze; 600 L/mm, 500 nm blaze; and 300 L/mm, 1200 nm blaze. ANDOR Newton (DU920-BV for the visible range) and iDUS (DU490A-1.7 for the NIR) detector heads were mounted at the exit ports of the Shamrock 500 spectrometer. The system was operated using the ANDOR Solis spectroscopy software. Detector heads were cooled to $-90 \text{ }^\circ\text{C}$, the spectrometer was purged with dry N_2 , and the detection system was calibrated with NIST traceable lamps as described elsewhere.^{25,27,28}

UV–vis absorption spectra were determined using a Shimadzu spectrophotometer UV-2101PC. Electrochemical measurements were performed using acetonitrile and butyronitrile solvents, tetrabutylammonium hexafluorophosphate electrolyte, and a BAS 100B electrochemical system. ^1H NMR spectra ($\delta = 3.60\text{--}2.05 \text{ ppm}$; m, 26 H) were obtained in d_6 -acetone and DMSO using a Varian 400 MHz instrument.

Procedures. Complexes were irradiated in their MLCT absorption bands using the following: a 532 (50 mW) and 470 nm (5 mW) CW diode MGL-S-B laser modules (Changchun Industries Optoelectronics Tech Co. Ltd.) purchased from OnPoint Lasers Inc.; a 405 nm (50 mW) CW diode laser module purchased from Power Technologies, Inc., Little Rock, AR. The calibrated spectral emission intensities^{28,56} were generated in units of photons per second. Emission amplitudes were determined by dividing the emission intensities at frequency ν_m by ν_m (see eq 1 below).^{20,60}

The 77 K emission spectra used samples in 2 mm cylindrical cells immersed in liquid N₂ in a Dewar as previously described.⁶¹ Ambient spectra and lifetimes were determined either in the 2 mm cell/Dewar system or with samples in 1 cm cuvettes. Sample solutions were prepared in butyronitrile for spectroscopic studies.

Computational Procedures. Our previous studies^{25,27,28} have suggested that the vibronic sideband amplitudes in the emission spectra of [Ru(L₄)bpy]^{m+} complexes vary with excited-state energy, but this inference was based on variations in the (L₄) ligands. In order to examine this hypothesis without the complications introduced by varying types of ancillary ligands, we modeled the effects of only variations in ³MLCT energy by changing the electrostatic charge at the Ru center (Z_{Ru}) but minimized variations in other factors by restricting our calculations to the [Ru(NH₃)₄bpy]²⁺ complex. Variations in Z_{Ru} change the donor ability (or oxidation potential) of the Ru center. We chose [Ru(NH₃)₄bpy]²⁺ as the model complex because of its simple sigma-donor ancillary ligands which make minimal contributions to the frontier orbitals.⁵⁴ It is important to emphasize that the adjustable nuclear charge (Z_{Ru}) in our model is not an effective nuclear charge (Z_{eff}) for any specific complex, but its variations do simulate the variations in Z_{eff} that are induced by the ancillary ligands. Varying Z_{Ru} from 43.5 to 44.5 allowed us to probe emission energies between ~5000 and 20 000 cm⁻¹, covering the range observed experimentally by means of ancillary ligand variations. Our calculations that simulated the emission spectra and band shapes of the [Ru(NH₃)₄bpy]²⁺ and [Ru(CH₃CN)₄bpy]²⁺ complexes (Figure 3) used the normal value of $Z_{Ru} = 44.0$.

Electronic structure calculations were carried out using DFT⁶² as implemented in a developmental version of Gaussian.⁶³ In previous reports on the absorption spectra of related polypyridine Ru complexes,^{54,64} we tested a number of modeling approaches and found that the B3PW91 functional^{32–35} in combination with the SDDall basis set^{65–67} produced good correlation with experiment for a modest cost. In this report we employ the more flexible D95V basis set for main group atoms for a better description of the molecular geometries.⁶⁶ Wave functions were tested for SCF stability,^{68,69} and all optimized structures were confirmed as minima by analyzing the harmonic vibrational frequencies.⁷⁰ The ground-state singlet (S_0) and triplet (T_0) dication states and reduced doublet [Ru^{II}(NH₃)₄bpy^{•+}]⁺ were computed with standard SCF methods, and analytic frequencies were obtained for each. The excited-state singlet (S_1) was computed using TD-DFT methods. Both of the “excited” states, T_0 and S_1 , were optimized starting from the optimized S_0 geometry. In addition, we optimized the S_1 geometry starting from the optimized T_0 geometry, and both calculations converged to the same structure. Finally, we also optimized the T_0 structure using TD-DFT, and the structure agrees well with the one obtained with Δ SCF (see Supporting Information S2).⁵⁹ Solvation effects (in acetonitrile) were accounted for using the most recent implementation of the implicit IEF-PCM solvation model (see Supporting Information S3),^{59,71–74} and were included during structure optimization. Isodensity plots of orbitals were visualized using GaussView.⁷⁵ Vibrationally resolved emission spectra were computed within the Franck–Condon approximation as implemented in Gaussian by Barone et al.^{51–53,76} Default parameters were employed except the full-width at half-height (fwhh) was increased to 400 cm⁻¹ for the Gaussian band shapes of individual Franck–Condon transitions.

RESULTS

A. Variations in Observed Emission Band Shapes of [Ru(X)₄bpy]^{m+} Complexes. 1. *Emission Spectra at 77 K of [Ru(CH₃CN)₄bpy]²⁺, [Ru([14]aneS₄)bpy]²⁺, and [Ru(acac)₂bpy].* These complexes were prepared for this study because we expected their emission energies to be higher and lower, respectively, than those previously reported, thereby enabling a comparison of the computational modeling with an extended range of emission band shapes; see Figure 2 and

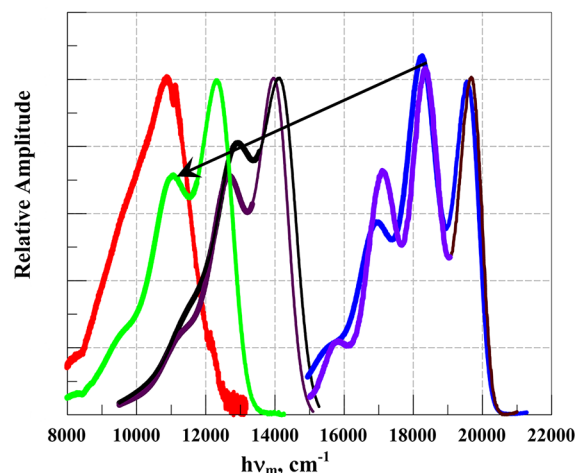


Figure 2. Emission (77 K) spectra of some [Ru(L₄)bpy]^{m+} complexes. From left to right, L₄ = (acac)₂, red; (NH₃)₄, green; [14]aneN₄, red brown; Me₂pyo[14]eneN₄ (*meso*-2,12-dimethyl-3,7,11,14-tetraazabicyclo[11.3.1]heptadeca-1(17),13,15-triene), black; [14]-aneS₄, lavender; (CH₃CN)₄, blue. Arrow indicates the general trend in the *mf* vibronic sideband amplitudes. Spectral amplitudes have been adjusted so that the highest energy emission bands have the same amplitudes and vibronic sidebands are approximately indicated by heavier lines in the spectral curves. Spectra of the tetraam(m)ine complexes are from Chen et al.²⁵

Table 1. The 77 K emission spectrum of [Ru(CH₃CN)₄bpy]²⁺ is at somewhat lower energy and broader in a frozen ethanol/methanol solution than in a butyronitrile glass. [Ru([14]-aneS₄)bpy]²⁺ emission was much weaker and had less than 0.4% of the lifetime of [Ru(CH₃CN)₄bpy]²⁺.

The vibronic sidebands in the spectra of [Ru(CH₃CN)₄bpy]²⁺ and [Ru([14]aneS₄)bpy]²⁺ are well resolved, and their relative amplitudes are the largest that we have found for any Ru–bpy complex. That the 77 K emission spectral band shapes of these two complexes are so similar in butyronitrile glasses demonstrates that their very large amplitude vibronic sideband contributions are associated with high energy of the ³MLCT excited states and not with vibronic contributions of their ancillary ligands. In contrast, the vibronic sidebands are not resolved in the 77 K emission spectrum of [Ru(acac)₂bpy], and the spectral band shapes of the [Ru(tetraam(m)ine)bpy]²⁺ complexes²⁵ fall between these limits (Figure 2).

2. Some General Aspects of Vibronic Sideband Contributions. The emission spectrum can be represented as the sum of contributions from the band origin ($E^{0/0}$ component; $j = 0$ in eq A2 in the summary of the basic structure of the Franck–Condon factors in the Appendix) and the vibronic sideband components that arise from excited-state distortions. For our purposes it is useful to express the emission spectrum of a

Table 1. Spectroscopic and Electrochemical Properties of Some [Ru(L)₄bpy]^{m+} Complexes

(L) ₄	absorption ^a		electrochemistry ^b			observed 77 K emission maxima ^{a,c}			calculated emission maxima ^{a,d}		
	$h\nu_{\max}(\text{obsd})$	$h\nu_{\max}(\text{H}_0/\text{L}_0)^d$	$E_{1/2}(\text{Ru}^{\text{III/II}})$	$E_{1/2}(\text{bpy})$	$F\Delta E_{1/2}^a$	highest energy	second highest energy	$\Delta h\nu_{\max}$	highest energy ^e	second highest energy	$\Delta h\nu_{\max}$
(acac) ₂	16 100 ^f	12 900 ^f	0.05	~−1.8	14 900	10 800 ^g					
(NH ₃) ₄	18 863 ^h	15 500 ^h	0.69 ^h	−1.56 ^h	18 100	12 400 ^h	11 100 ^h	1300	11 800	10 400	1400
(CH ₃ CN) ₄ ^g	25 270	23 300	1.66	−1.44	25 000	19 400	18 000	1400	18 600	17 200	1400
[14]aneS ₄ ^g	24 970		1.56	−1.27	23 600	19 600 ⁱ	18 200 ⁱ	1400			
						19 680	18 390	1290			

^aEnergies in units of cm^{−1}. ^bHalf-wave potentials in units of V vs SSCE; referenced to $E_{1/2}(\text{Fc}^{0+}) = 0.367$ V vs SSCE (internal ref). ^cButyronitrile glass except as indicated. ^dCalculated for the T₀ → S₀ transition. ^eCalculated HOMO → LUMO transition energy (B3PW91/SDDall). ^fAllard et al.^{54,77} ^gThis work. ^hChen et al.²⁵ ⁱEthanol/methanol glass

donor/acceptor complex as (see also eqs A1 and A4 in the Appendix)^{19,20,78,79}

$$I_{\nu_m(\text{exp } t)} \approx \nu_m H_{\text{eg}}^2 \Delta \mu_{\text{eg}}^2 B(\gamma_{0'0} G_{\nu_m(0'0)} + \gamma_{\text{sb}} V_{\nu_m}) \quad (1)$$

where $G_{\nu_m(0'0)}$ is a Gaussian representing the shape of the $E^{0'0}$ component and V_{ν_m} is the shape of the envelope of vibronic contributions. The weighting factors in eq 1, $\gamma_{0'0}$ and γ_{sb} , meet the condition that^{11,52}

$$\int_{\nu_m} \frac{I_{\nu_m(\text{exp } t)}}{\nu_m} d\nu_m = 1 \quad (2)$$

For the complexes considered here there are distortions in many vibrational modes and the vibronic envelope must contain sums of the progressions in each of these modes and of the vibronic progressions involving different normal modes (combination bands). Computational evaluation of the vibronic contributions is organized in terms of single-mode progressions (ν_k , ν_k^2 , ν_k^3 + ... + ν_k^j) and combination bands. Expressed in this manner

$$V_{\nu_m} = \sum_k A_{\nu_m k} \approx A_{\nu_m(\text{bpy})} + A_{\nu_m(\text{ML})} + A_{\nu_m(\text{OT})} \quad (3)$$

In this representation, the vibrational modes with fundamentals in the $1000 \leq \nu_k/\text{cm}^{-1} \leq 1600$ (*mf*) range arise largely from bpy distortions and those in the $\nu_k/\text{cm}^{-1} < 800$ (*lf*) range are largely metal–ligand modes (ML). The $A_{\nu_m(\text{OT})}$ term for the Ru–bpy complexes contains spectral sideband contributions other than those that give rise to the single-mode progressions of predominately bpy or metal–ligand vibrational modes, such as combination bands and ancillary ligand modes. Combination bands can be represented as sums for the various distortion modes, $\nu_k = a\nu_p + b\nu_q + c\nu_r + \dots$, for $j = (a + b + c + \dots)$ combinations where $p \neq q \neq r$, etc., and for the second-order combination bands

$$A_{\nu_m(\text{C})} = \sum_{k=p \neq q} \sum_{k=q} A_{\nu_m(k)} \quad (4)$$

Since there are more than 10 active distortion modes in the complexes considered here,^{12–14,18–20} there are a very large number of combination bands (>10² second order; >10³ third order; etc.). An important factor in the resolution of the vibronic sidebands is the bandwidth (fwhh) of the spectral components,²⁸ and the fwhh is qualitatively manifested in the slope of the rise in spectral intensity on the high-energy sides of the emission spectra. Thus, the [Ru(CH₃CN)₄bpy]²⁺ complex appears to have the smallest while the [Ru(acac)₂bpy] complex appears to have the largest component bandwidth of the

complexes considered in Figure 2. The [Ru(ethyl-2-chlorotrifluoroacetoacetate)₂bpy] and [Ru(1,1,1-trifluoropentane-2,4-dione)₂bpy] complexes also emit at relatively low energies and have relatively large bandwidths (Supporting Information Figure S4).⁵⁹ Our computational modeling indicates that there are distortions in several *lf* vibrational modes and that these tend to dominate the spectra of complexes that emit at lower energies. Consequently, differences in the slopes of the high-energy rise in spectral intensity are not necessarily proportional to differences in component fwhh, and the increased contributions of these *lf* modes will effectively broaden the vibronic bands of the higher frequency vibronic components.

We have previously observed that the amplitudes of the vibronic sidebands of Ru–bpy complexes tend to decrease systematically as the energies of the MLCT excited states decrease.^{25,27,28,80} Since there are so many distortion modes, some of the observed differences in sideband contributions, illustrated in Figure 2, can arise from variations in the overlapping vibronic contributions in complexes with different component bandwidths.²⁸ In addition, the *lf* vibronic components vary appreciably with the ancillary ligands, and the harmonics and combination bands that result from these *lf* contributions will also contribute amplitude in the 1000–1600 cm^{−1} region to further complicate interpretation of the observed spectral vibronic sidebands (see the computed examples in Figure 4 below).^{27,28} The [Ru([14]aneN₄)bpy]²⁺ and [Ru(Me₂pyo[14]eneN₄)bpy]²⁺ (data from Chen et al.;²⁵ see Supporting Information S5 for ligand structures)⁵⁹ emission spectra included in Figure 2 illustrate contrasting vibronic sideband contributions that arise from some combination of these contributions. That no vibronic sidebands are resolved in the spectrum of the [Ru(acac)₂bpy] complex most likely arises from the combined effects of (a) very large component bandwidths, (b) substantial ancillary ligand vibronic contributions, and (c) the weak bpy vibronic contributions that are associated with low-energy emission spectra. Some ancillary ligand contributions are expected since the HOMO calculated for [Ru(acac)₂bpy] contains about 8% acac character, while ancillary ligand contributions to the respective HOMOs are small for [Ru(CH₃CN)₄bpy]²⁺ and much smaller for [Ru(NH₃)₄bpy]²⁺.⁵⁴

3. Computational Simulation of Emission Spectra. We computed the T₀ excited-state energies and structures at the B3PW91/SDD level of theory in order to calculate the emission spectra of the [Ru(NH₃)₄bpy]²⁺ and [Ru(CH₃CN)₄bpy]²⁺ complexes (Figure 3). The calculated spectra underestimate the energy of the first emission feature by about 500 and 1000 cm^{−1}, respectively. In both cases the calculations

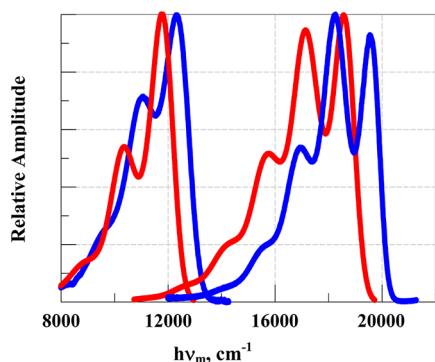


Figure 3. Comparison of the observed (butyronitrile solvent at 77 K) (blue) and calculated (IEF-PCM) (red) emission spectra of $[\text{Ru}(\text{NH}_3)_4\text{bpy}]^{2+}$ (left) and $[\text{Ru}(\text{CH}_3\text{CN})_4\text{bpy}]^{2+}$ (right).

underestimate the relative amplitudes of the first vibronic feature, and this is probably because (a) we use an implicit solvation model instead of explicitly including the butyronitrile glass, (b) we treat the *lf* ML modes as harmonic, (c) the excited-state energies are underestimated and the *mf* vibronic envelopes are expected to be somewhat larger at the observed energies (see Figures 2 and 3 and the discussion below), and (d) the bandwidths used in the calculations are not fully optimized to fit the spectra.

B. Computational Modeling of the Energy-Dependent $^3\text{MLCT}$ Excited-State Distortions in the Ru/bpy Chromophores. 1. *Variations in the Band Origin ($E^{0/0}$) and Relative Importance of Low-Frequency Vibronic Components.* The calculations indicate that the band origin components ($E^{0/0} = \langle 0' | 0 \rangle$) make relatively small contributions, less than 50% to the highest energy emission feature of both $[\text{Ru}(\text{NH}_3)_4\text{bpy}]^{2+}$ and $[\text{Ru}(\text{CH}_3\text{CN})_4\text{bpy}]^{2+}$ (see Figures 3 and 4), and that most of the amplitude of the highest energy features should be attributed to vibronic contributions of *lf* Ru–N deformation modes. Increases in these *lf* contributions will necessarily reduce the relative (or percentage) spectral contributions of the *mf* distortion modes and potentially complicate assessment of

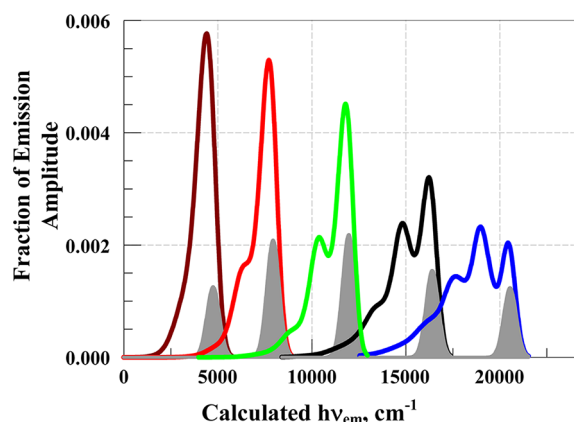


Figure 4. Calculated emission spectra of $[\text{Ru}(\text{NH}_3)_4\text{bpy}]^{2+}$ for a range of $^3\text{MLCT}_0$ excited-state energies. Calculated emission spectra are normalized so that the integrated area of each spectrum is 1; gray Gaussian component of each spectrum corresponds to the calculated band origin ($E^{0/0}$) component. Energies correspond to the values of Z_{Ru} used in the calculations: 43.50, burgundy; 43.75, red; 44.00, green; 44.25, black; 44.50, blue. Spectra are programmatically constructed from the calculated vibronic components presented in Figures 6–8.

the variations in their contributions. Consequently, it is gratifying that the computational results support the inference based on the observed band shapes that the amount of bpy distortion in the tetrakis-acetonitrile complex is larger than that in the tetraammine. For example, the computed C1–C1' bond lengths of the ground and the $^3\text{MLCT}_0$ excited states differ by 0.061 Å (1.465 → 1.404 Å) and 0.048 Å (1.459 → 1.411 Å), respectively. However, changing the ancillary ligands can result in vibronic contributions from those ligands, differences in metal–ligand σ/π bonding, complex–lattice interactions, etc., and the contributions of these differences could complicate determination of the extent to which emission band shapes vary with excited-state energy.

We directly addressed the question of how the emission band shapes vary when only the excited-state energy changes by calculating the variations in excited-state distortions with changes in the adjustable nuclear charge for Ru (Z_{Ru}) from 43.5 to 44.5 in $[\text{Ru}(\text{bpy})(\text{NH}_3)_4]^{2+}$ (thus, holding all other coordination sphere parameters constant) and reoptimizing the structures of S_0 and T_0 for each value of Z_{Ru} using the B3WP91 functional with the SDD and D95V basis sets. Vibronic components calculated for each value of Z_{Ru} were assumed to have Gaussian band shapes (fwhh = 400 cm^{-1}), and these were combined with the appropriate calculated $E^{0/0}$ component to produce the spectra in Figure 4.

These calculated spectra indicate that (1) distortions in bpy modes decrease with the MLCT excited-state energy and their relative contributions nearly disappear at very low energies, (2) low-energy vibrational modes contribute significantly to the emission spectral band shape and their relative contribution increases as the MLCT excited-state energy decreases, and (3) the contributions of the $E^{0/0}$ components (solid gray Gaussians of Figure 4) range from minimum spectral contributions of about 13% at the highest and lowest energies considered to about 23% in the middle of the range.

2. *Energy Contributions to the $S_0 \rightarrow S_1$ and $T_0 \rightarrow S_0$ Transitions in $[\text{Ru}(\text{NH}_3)_4\text{bpy}]^{2+}$.* The vertical $S_0 \rightarrow S_1$ and $S_0 \rightarrow T_0$ transition energies can be separated into contributions of (a) the respective differences in the energies of the ground- and excited-state PE minima ($E^{0/0}$ components in Figure 4 for the latter) and (b) the reorganizational energies $\lambda_{S(1)}$ and $\lambda_{S(0)}$, respectively, that derive from the excited-state distortions (see Figure 1). Our modeling indicates that $\lambda_{S(1)} \approx \lambda_{S(0)} \approx 1400 \text{ cm}^{-1}$. The energy difference between the S_1 and the T_0 PE minima corresponds to an exchange energy ($2K_{\text{exch}}$) in the diabatic limit, but it is more complicated in the adiabatic systems, and our computational model for this complex yields $\Delta E_{\text{ST}} \approx 1800 \text{ cm}^{-1}$. These are all relatively small numbers. Detailed calculations further indicate that there is a difference in the S_1 and T_0 distortions, with distortions in *lf* modes making larger and the *mf* modes making smaller relative contributions to $\lambda_{S(1)}$ than to $\lambda_{S(0)}$ (see Supporting Information S6).⁵⁹

3. *DFT-Calculated Vibronic Distortions.* The vibronic contributions to the calculated $[\text{Ru}(\text{NH}_3)_4\text{bpy}]^{2+}$ $^3\text{MLCT}$ emission spectra are spread over a wide vibrational frequency range, and assessing the patterns of the contributing distortions is difficult because (1) the calculations indicate that the distortions in the *lf* and *mf* modes vary differently as the excited-state energy increases contrary to the expectation that the distortion amplitudes would vary in unison if they arose from a single source such as transfer of an electron from Ru to bpy and (2) the contributions of higher order vibrational modes vary a great deal through the range of energies

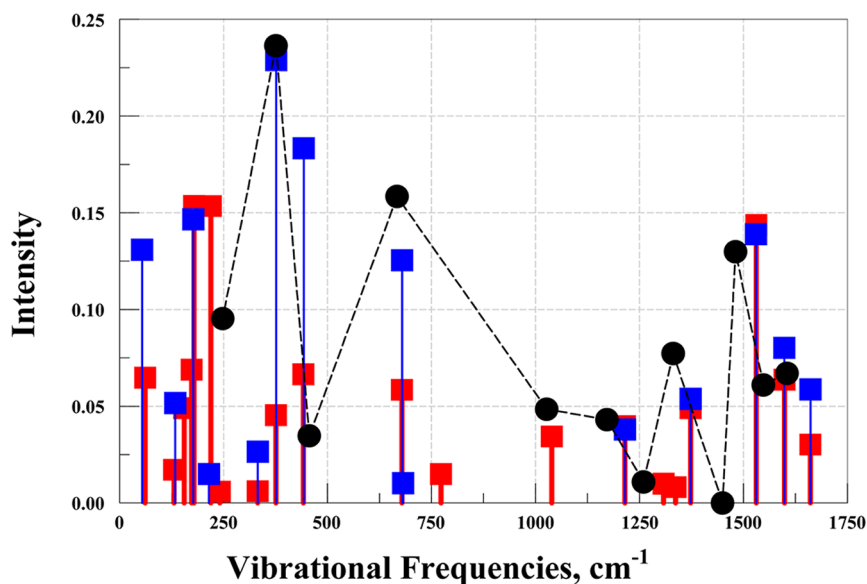


Figure 5. Comparison of the relative intensities of rR vibronic components (black circles connected by dashed lines) and those calculated (B3PW91 with SDD and D95V basis sets) for the S_1 (blue squares) and T_0 (red squares) excited states of $[\text{Ru}(\text{NH}_3)_4\text{bpy}]^{2+}$. Relative intensities for the rR components are based on $S_k e^{-S_k}$, and those calculated for S_1 and T_0 are arbitrarily adjusted for a reasonable match in the 1000–1700 cm^{-1} range; values of S_k are from Hupp and Williams.²²

considered. We previously used the vibronic parameters from rR spectra as a basis for modeling the vibronic structure of Ru–bpy emission spectra,^{27,28} but the rR probes the singlet manifold and the transition to the $^1\text{MLCT}(S_1)$ excited state of $[\text{Ru}(\text{NH}_3)_4\text{bpy}]^{2+}$ apparently has a very small oscillator strength,⁵⁴ so the states probed by rR are most likely upper states whose distortions probably differ from those of S_1 .

Correlations of the bpy ligand distortions to the amount of charge transferred have been recently discussed by Scarborough and Wieghardt,²¹ and in order to better model the origins of the large variations in vibronic sidebands, we calculated the excited-state bpy–ligand bond-length changes that are expected to accompany variations in the excited-state energies.

a. Comparison of First-Order Vibronic Intensities Calculated for S_1 and T_0 with Those Based on Resonance-Raman Spectra. Figure 5 shows the relative intensities of first-order vibronic components calculated for the S_1 and T_0 excited states of $[\text{Ru}(\text{NH}_3)_4\text{bpy}]^{2+}$ and compares them to the first-order vibronic intensities ($F_{j=1} = e^{-S}S$ from eq A3) based on the Huang–Rhys parameters obtained from the rR spectrum²² with their amplitudes adjusted uniformly for reasonable agreement with calculations in the mf regime. In our calculations the transition dipole moment integral (TDMI) is assumed to be one for $T_0 \rightarrow S_0$ since that is a spin-forbidden transition, and therefore, we scaled the $T_0 \rightarrow S_0$ vibronic components by the $(\text{TDMI})^2$ for $S_1 \rightarrow S_0$, so that all else being equal, they would have similar magnitudes. The rR frequencies appear to be consistently 3% smaller in the 1000–1700 cm^{-1} range of bpy distortion modes than are the calculated frequencies of the S_1 or T_0 excited-state distortion modes, but otherwise, the relative variations in amplitude are similar in the mf regime. There are a few differences in this vibronic regime that may be significant: (a) there appears to be a relatively larger overall distortion of T_0 than S_1 in the highest frequency modes (see also Supporting Information S7) and (b) the distortion in the component at about 1030 cm^{-1} in the T_0 excited state and in the rR spectrum appears to be absent from the calculated S_1 vibronic components (see Supporting Information S8 for the calculated

distortion modes).⁵⁹ Despite the differences of detail, Figure 5 and the previous observation²⁶ that the rR active mf vibrational modes of $[\text{Ru}(\text{NH}_3)_4\text{bpy}]^{2+}$,²² $[\text{Ru}(\text{bpy})_3]^{2+}$,²³ and $[\text{Os}(\text{bpy})_3]^{2+24}$ are remarkably similar in frequency (see also Supporting Information Table S8)⁵⁹ and relative amplitude supports the proposed use of the rR parameters to model bpy ligand distortions in MLCT excited states. The overall relative agreement between computed and rR-based vibronic intensities in this region leads to nearly superimposable envelopes of the mf components when component bandwidths appropriate to the frozen solution spectra are used as is illustrated in Figure 6. Furthermore, the overall agreement of rR-based and computed vibronic band shapes in the mf regime is good support for the computational modeling reported here.

The relatively large distortions in the metal–ligand modes that result from the DFT spectral modeling implies some complications in the analyses of experimental emission band shapes: (a) the band origin ($E^{0/0}$) component makes relatively small spectral contributions (see Figure 4) and is difficult to identify in the experimental spectra, and (b) these lf modes would complicate the evaluation of distortions in the mf vibronic regime of experimental spectra due to the overlapping of contributions from their vibronic progressions and combination bands (discussed in the following section). On the other hand, the lowest energy calculated vibronic component is on the order of $k_B T$ at 77 K and would probably appear as a bandwidth contribution in our experimental spectra. Along the same lines, the metal–ligand distortion modes which have fundamental vibrational frequencies less than about 200 cm^{-1} would appear as bandwidth contributions in ambient emission spectra and may not be resolvable in rR spectra.

b. Comparisons of the Modeled (B3PW91 with SDD and D95V basis sets) bpy Ligand Distortion Amplitudes of Ru–bpy $^3\text{MLCT}$ Excited States. Figure 7 compares the variations in the calculated component contributions to the calculated spectra shown in Figure 4. The middle panel in Figure 7 shows the envelopes of calculated single vibrational mode

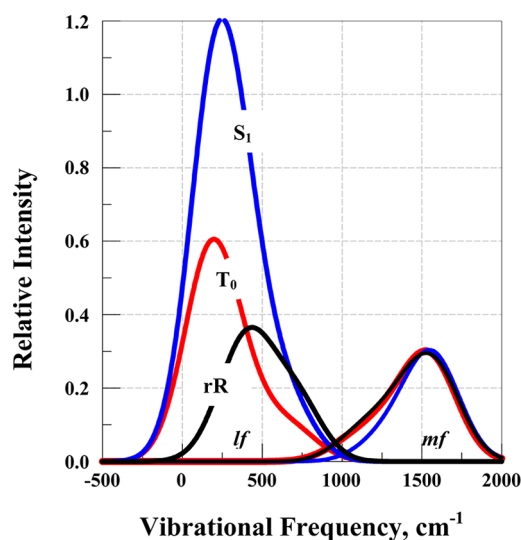


Figure 6. Comparison of the relative first-order calculated (DFT) and rR vibronic contributions ($j = 1$ in eq A3) to the intensity of the emission band shape of $[\text{Ru}(\text{NH}_3)_4\text{bpy}]^{2+}$ for $S_1 \rightarrow S_0$, blue, $T_0 \rightarrow S_0$, red, rR, black. Gaussian component band shapes were used for this comparison with $\text{fwhm} = 372 \text{ cm}^{-1}$, intensities were adjusted so that the mf envelopes had the same maximum amplitudes, and frequencies of the rR modes were increased by 50 cm^{-1} .

contributions which correspond largely to $A_{\nu_m(\text{bpy})}$ and $A_{\nu_m(\text{ML})}$ in eq 3.

The calculated variations of the total (or integrated) contributions of the $E^{0/0}$ component, progressions in first-order distortion modes, and combination bands to the emission spectra as a function of the $E^{0/0}$ energies of the spectra in Figure 4 are shown in Figure 8. The dominant vibronic peaks in the envelopes of the combination band contributions (Figure 7) occur consistently at vibrational frequencies of about 620, 1830, and 2830 cm^{-1} in the calculated spectra. These frequency ranges correspond mostly to combinations of $(\nu_i(\text{ML}) + \nu_j(\text{ML}))$, $(\nu_k(\text{ML}) + \nu_m(\text{bpy}))$, and $(\nu_p(\text{bpy}) + \nu_q(\text{bpy}))$ vibrational modes, respectively, where $\nu_i \neq \nu_j$ and $\nu_p \neq \nu_q$. The fact that the $(\text{bpy} + \text{bpy})$ combination bands make a larger contribution than the combination bands involving ML vibrational modes for the highest energy ${}^3\text{MLCT}_0$ excited state indicates that the internal distortions of the bpy ligand are greater than the distortions in the metal–ligand vibrational modes and that distortions in the bpy ligand vibrational modes do increase as the excited-state energy increases. Similarly, the very large contribution of $(\text{ML} + \text{ML})$ and the near absence of $(\text{bpy} + \text{bpy})$ combination bands in the lowest energy calculated emission spectrum of Figure 4 (see also the middle panel of Figure 7) indicates that the distortion of this excited state is mostly in the metal coordination sphere. The fact that the calculated combination band contributions go through a minimum at $E^{0/0} \approx 14\,000 \text{ cm}^{-1}$ suggests that the ML and bpy distortions arise from variations in the orbital compositions of the electronic excited states through the energy range considered.

c. Variations of Structural Parameters Calculated for Ground and Excited States with Z_{Ru} . The simulated and observed emission spectra discussed above indicate that the emission band shapes are strong functions of the excited-state energy. Since the variations in vibronic sideband amplitudes imply variations in excited-state structures, we also computa-

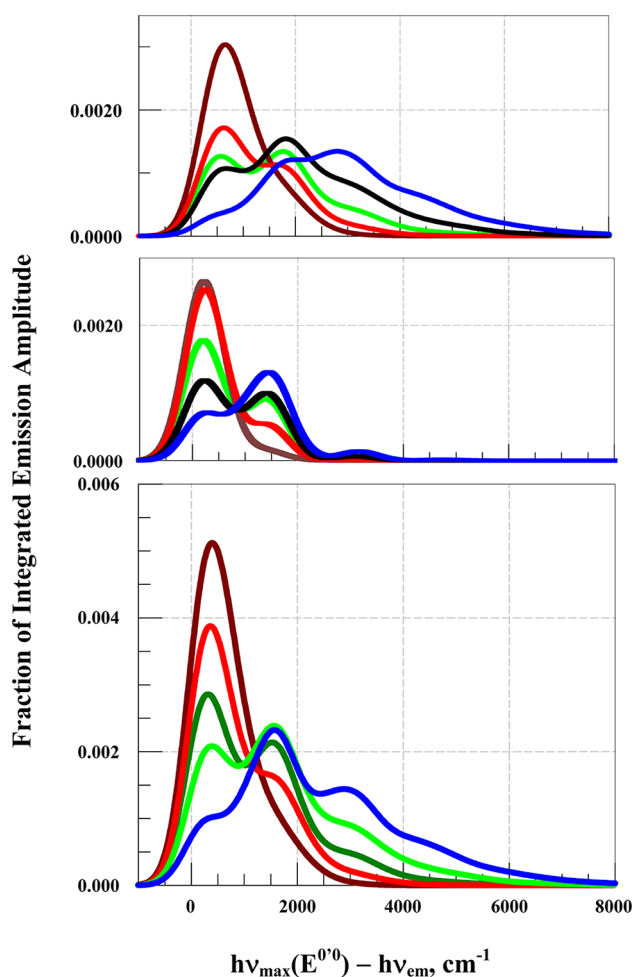


Figure 7. Comparisons of the calculated envelopes of the vibronic contribution (to 7th order) for different values of Z_{Ru} in $[\text{Ru}(\text{NH}_3)_4\text{bpy}]^{2+}$ (colors of the envelopes are selected to match those in Figure 4). Vibronic envelopes are presented on the scale of vibrational frequencies. Areas of the respective envelopes correspond to their fractional contributions to the emission spectra in Figure 4. Lower panel shows the total vibronic sideband contributions; upper panel contains the calculated progressions in single vibrational modes; and upper panel contains the calculated envelopes of combination band contributions to the spectra in Figure 4.

tionally examined the differences between these structures and those of the ground states based on $[\text{Ru}(\text{NH}_3)_4\text{bpy}]^{2+}$ parameters by varying Z_{Ru} . Thus, we modeled the ground state of this complex, its ${}^3\text{MLCT}_0$ and ${}^1\text{MLCT}_1$ excited states, and the doublet ground state of $[\text{Ru}(\text{NH}_3)_4\text{bpy}^{\bullet-}]^{1+}$ over a range of hypothetical excited-state energies. The results are summarized in Table 2 and Figure 10. Scarborough and Wiegardt proposed that the lengths of the $\text{C}_1-\text{C}_1'$ and N_b-C_1 bonds (see Figure 9 for atom labels) in a bpy ligand can be correlated with its oxidation state (or charge).²¹ We compared this proposal to the bond lengths calculated for hypothetical $[\text{Mg}(\text{NH}_3)_4\text{bpy}]^{2+/+}$ and $[\text{Al}(\text{NH}_3)_4\text{bpy}]^{3+/2+}$ species that are comparable in ionic radius to $[\text{Ru}(\text{NH}_3)_4\text{bpy}]^{2+/+}$ and other monobpy complexes examined in this study. These calculated bond lengths are also summarized in Table 2. The calculated $\text{C}_1-\text{C}_1'$ $[\text{Mg}(\text{NH}_3)_4\text{bpy}]^{2+}$ and $[\text{Al}(\text{NH}_3)_4\text{bpy}]^{3+}$ bond lengths (1.486 and 1.476 Å, respectively) are somewhat shorter (and just outside the reported uncertainties) than reported for $[\text{Al}(\text{bpy})_3]^{3+}$ ($1.490 \pm 0.003 \text{ Å}$) and somewhat longer than

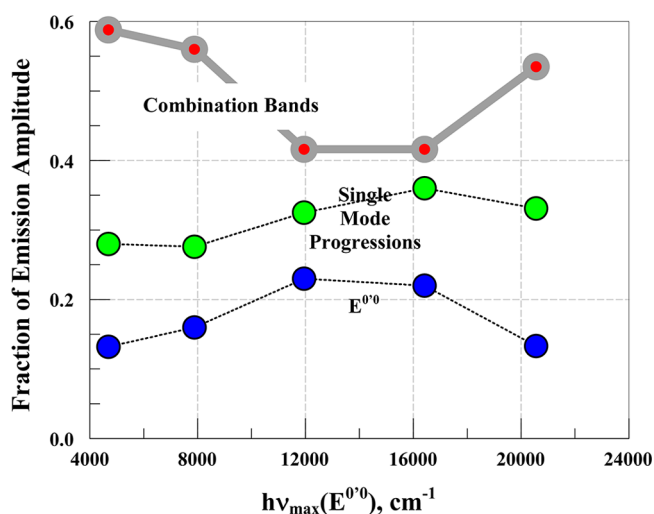


Figure 8. Comparison of the calculated fractional contributions of the band origin ($E^{0/0}$; blue), progressions in single vibrational modes (vibrational fundamental and harmonics; bright green), and combination bands (gray) to the emission spectra calculated (with $\text{fwhm} = 400 \text{ cm}^{-1}$) for $[\text{Ru}(\text{NH}_3)_4\text{bpy}]^{2+}$ for the different excited-state energies shown in Figure 4. Note that these relative contributions are bandwidth dependent.²⁸

those found for $[\text{Ru}(\text{NH}_3)_4\text{bpy}]^{2+}$ in the X-ray crystal structure ($1.475 \pm 0.005 \text{ \AA}$)²⁵ and the calculated values (1.465 \AA). The $\text{C}_1\text{--C}_1'$ bond lengths of all the metal–bpy complexes considered are shorter than that calculated for the free, planar bpy ligand.

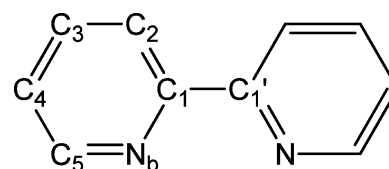


Figure 9. Atom-numbering scheme for the bipyridine ligand.

For the smallest values of Z_{Ru} considered, the $\text{C}_1\text{--C}_1'$ and Ru--N_b bond lengths calculated for the $[\text{Ru}(\text{NH}_3)_4\text{bpy}]^{2+}$ ground state are relatively short and consistent with appreciable delocalization of an electron between Ru^{II} and bpy (Figures 10 and 11; see Discussion below). In the limit that the transferring electron has the same energy on Ru and bpy, (a) there would be only a small difference in the net electron density on the bpy ligand in the S_0 and T_0 electronic states ($\sim 25\%$), consistent with the trend toward smaller mf vibronic sidebands at the lowest energies in Figure 4, and (b) the S_0 and T_0 electronic states will involve different distributions of electron density among the $d\pi(\text{Ru})$ orbitals and therefore appreciable changes in metal–ligand bond lengths.

The Ru--NH_3 bond lengths calculated for the S_0 and T_0 electronic states of $[\text{Ru}(\text{NH}_3)_4\text{bpy}]^{2+}$ and $[\text{Ru}(\text{NH}_3)_4(\text{bpy}^{\bullet-})]^{2+}$ all decrease monotonically with Z_{Ru} and they are mostly smaller than the corresponding bond lengths calculated for $[\text{Mg}(\text{NH}_3)_4\text{bpy}]^{2+}$ and longer than those calculated for $[\text{Al}(\text{NH}_3)_4\text{bpy}]^{3+}$ consistent with the expected effects of metal charge on the bond length (see Table 2). Similarly, reduction of the coordinated bpy ligand of the Mg and Al complexes is calculated to result in about a 0.058 \AA shorter $\text{M--N}(\text{bpy})$ bond length. The calculated differences between Ru--

Table 2. Calculated Ground- and Excited-State Structural Parameters

state	Z_{Ru}	metal–ligand bond lengths ^a					bipyridine bond lengths ^a				
		M--N_{ax}	M--N_{eq}	M--N_b	$\text{N}_b\text{--C}_1$	$\text{C}_1\text{--C}_1'$	$\text{C}_1\text{--C}_2$	$\text{C}_2\text{--C}_3$	$\text{C}_3\text{--C}_4$	$\text{C}_4\text{--C}_5$	$\text{C}_5\text{--N}_b$
S_0 ($^1[\text{Ru}^{\text{II}}(\text{NH}_3)_4\text{bpy}]^{2+}$)	43.5	2.164	2.211	2.006	1.398	1.453	1.407	1.397	1.412	1.391	1.378
	43.75	2.155	2.194	2.020	1.389	1.459	1.406	1.398	1.409	1.394	1.371
	44	2.145	2.176	2.035	1.383	1.465	1.404	1.399	1.406	1.396	1.365
	44.25	2.134	2.159	2.048	1.378	1.469	1.403	1.400	1.404	1.397	1.361
	44.5	2.123	2.143	2.056	1.376	1.470	1.402	1.400	1.403	1.397	1.358
T_0 ($^3\text{MLCT};$ $^3[\text{Ru}^{\text{III}}(\text{NH}_3)_4\text{bpy}^{\bullet-}]^{2+}$)	43.5	2.151	2.190	2.058	1.414	1.418	1.432	1.383	1.431	1.389	1.368
	43.75	2.139	2.178	2.051	1.413	1.419	1.430	1.383	1.431	1.386	1.369
	44	2.129	2.168	2.041	1.413	1.418	1.429	1.382	1.432	1.384	1.371
	44.25	2.122	2.160	2.027	1.416	1.414	1.429	1.380	1.434	1.382	1.373
	44.5	2.117	2.149	2.017	1.430	1.400	1.439	1.375	1.436	1.390	1.362
D^+ ($^2[\text{Ru}^{\text{II}}(\text{NH}_3)_4\text{bpy}^{\bullet-}]^{2+}$)	43.5	2.169	2.225	2.021	1.432	1.415	1.434	1.388	1.431	1.398	1.369
	43.75	2.159	2.206	2.033	1.422	1.420	1.433	1.387	1.429	1.397	1.365
	44	2.147	2.189	2.043	1.416	1.423	1.432	1.386	1.428	1.396	1.362
	44.25	2.133	2.173	2.047	1.412	1.424	1.431	1.385	1.428	1.393	1.362
	44.5	2.120	2.159	2.046	1.410	1.424	1.430	1.384	1.429	1.390	1.363
(bpy) ⁰⁺ (planar)				1.362	1.498						
(bpy) ¹⁻				1.404	1.445						
$[\text{Mg}(\text{bpy})(\text{NH}_3)_4]^{2+}$	12	2.220	2.227	2.241	1.366	1.486	1.407	1.401	1.403	1.401	1.355
$[\text{Mg}(\text{bpy})(\text{NH}_3)_4]^{1+}$	12	2.237	2.245	2.183	1.405	1.436	1.435	1.386	1.430	1.394	1.360
$[\text{Al}(\text{bpy})(\text{NH}_3)_4]^{3+}$	13	2.057	2.066	2.056	1.371	1.476	1.401	1.401	1.402	1.396	1.359
$[\text{Al}(\text{bpy})(\text{NH}_3)_4]^{2+}$	13	2.081	2.085	1.997	1.406	1.429	1.425	1.384	1.430	1.382	1.374
X-ray structure for $[\text{Ru}^{\text{II}}(\text{NH}_3)_4\text{bpy}]^{2+}$ ^b		2.147(3)	2.159(3)	2.039(3)	1.358(4)	1.475(5)	1.393(5)	1.369(5)	1.389(5)	1.391(5)	1.350(5)
		2.133(3)	2.156(3)	2.046(3)	1.364(5)		1.385(5)	1.375(7)	1.383(7)	1.371(5)	1.346(5)

^aAbbreviations: N_{ax} = axial NH_3 ; N_{eq} = equatorial NH_3 ; N_b = $\text{N}(\text{bpy})$; atoms in 2,2'-bipyridine are abbreviated as in Figure 9. ^bData from Chen et al.²⁵

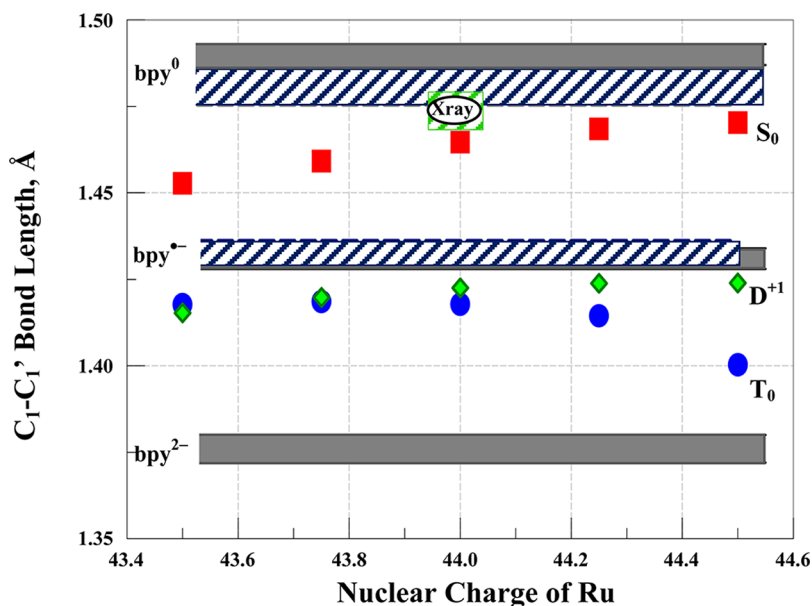


Figure 10. Graphical summary of the variations in the C_1-C_1' bpy-ligand bond lengths calculated with different Z_{Ru} for the $[Ru(NH_3)_4bpy]^{2+}$ ground (red squares; S_0), 3MLCT_0 (blue circles; T_0), and reduced doublet (green diamonds; D^+) states. Long solid gray bars correspond to the respective (X-ray-based) bond lengths reported for the noted oxidation states of the bpy ligand in $[Al(bpy)_3]^{3+}$ (from Scarborough and Wieghardt²¹ and references cited therein), where the bar heights correspond to the cited uncertainties. Gray hashed bars are the values calculated: (a) for the bpy ligand in $[Mg(NH_3)_4bpy]^{2+}$ and $[Al(NH_3)_4bpy]^{3+}$ (top and bottom, respectively, of upper bar) and (b) for the bpy ligand in $[Mg(NH_3)_4bpy]^+$ and $[Al(NH_3)_4bpy]^{2+}$ (top and bottom, respectively, of lower bar). Height of the green-hashed rectangle is based on the bond lengths and uncertainties found in the X-ray crystal structure of $[Ru(NH_3)_4bpy]^{2+}$.²⁵

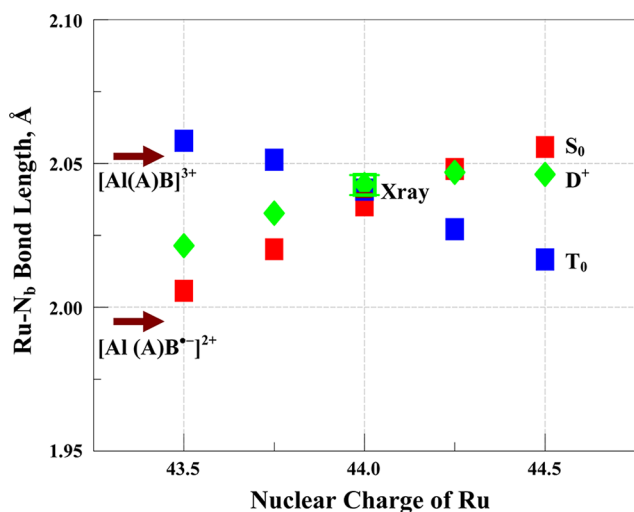


Figure 11. Calculated variations of the Ru–N(bpy) bond lengths with the Z_{Ru} in the $[Ru(NH_3)_4bpy]^{2+}$ ground state (S_0), $[Ru(NH_3)_4bpy]^{2+}$ triplet excited state (T_0), and reduced complex $[Ru(NH_3)_4(bpy^{\bullet-})]^+$ (D^+). Abbreviations: (A) = $(NH_3)_4$; B = bpy. Arrows indicate values calculated for $[Al(NH_3)_4bpy]^{3+}$ (upper) and its one-electron-reduced complex (lower). Green square indicates the value found in the X-ray crystal structure of $[Ru(NH_3)_4bpy]^{2+}$.²⁵

N(bpy) bond lengths for the S_0 , D^+ , and T_0 complexes are more interesting: for the S_0 and $[Ru(NH_3)_4(bpy^{\bullet-})]^+$ complexes Ru–N(bpy) increases while that of T_0 decreases monotonically with Ru-nuclear charge (Figure 11). This behavior does not conform to simple expectation based only on the shift in electrical charge of a simple MLCT excited-state model in which an electron has been transferred from Ru^{II} to bpy. However, the calculated variations in bond lengths are qualitatively consistent with the X-ray crystal structures of Ru^{II}

($Z_{Ru} = 44.0$) and with the Ru^{III} complexes with pyridine and related ligands.^{25,81}

Since the vibronic amplitudes are functions of the squared displacements (i.e., in λ_{vib} , eqs A1–A3) we presented the differences between the calculated S_0 and T_0 bond lengths squared in Figure 12. However, these are not modal displacements and the comparisons between the contributions to lf and mf vibrational modes are necessarily qualitative; the relative Ru–ligand/bpy Huang–Rhys parameters could be 3–5

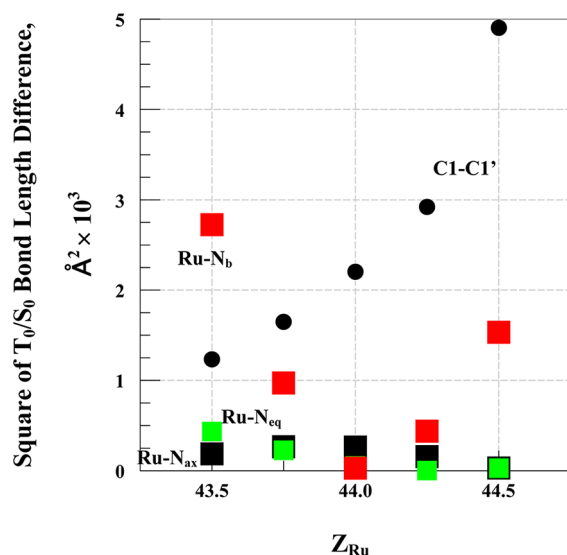


Figure 12. Variations in the squares of the differences between selected T_0 and S_0 bond lengths calculated for $[Ru(NH_3)_4bpy]^{2+}$ with different values of Z_{Ru} : equatorial Ru– NH_3 , green squares; axial Ru– NH_3 , black squares; Ru–N(bpy), red squares; C_1-C_1' , black circles.

times greater than indicated in Figure 12. Nevertheless, the overall trends are as outlined above and most of the variations in *lf* modes appear to arise from the strongly energy dependent, ancillary ligand-independent variations in the Ru^{II}–N(bpy) displacements, and consistent with the peculiar pattern of the variation in combination band amplitudes in Figure 8.

The calculated C₁–C₁' bond length decreases more than expected for a simple, Ru^{II}/bpy electron-transfer model of the MLCT excited state for the largest values of Z_{Ru} considered and is in contrast to the small increases in the C₁–C₁' bond lengths calculated for the [Ru(NH₃)₄(bpy^{•-})]⁺ complex (see Figure 10). Given the uncertainties in finding an appropriate reference for the limit of an extra electron localized on the bpy ligand of a ruthenium complex, the C₁–C₁' bond lengths calculated for [Ru(NH₃)₄(bpy^{•-})]⁺ are reasonably consistent with expectation for this limit based on the Al and Mg reference species. In contrast, the marked decrease in calculated C₁–C₁' bond lengths in T₀ structures for Z_{Ru} > 44.0 indicate appreciable strengthening of that bond for high-energy Ru/bpy MLCT excited states.

DISCUSSION

The [Ru(CH₃CN)₄bpy]²⁺ and [Ru([14]aneS₄)bpy]²⁺ complexes emit at higher energies (~20 × 10³ cm⁻¹) than other known monobpy Ru complexes and their *mf* (bpy-centered) vibronic (ν_{mf}) sidebands dominate the 77 K emission spectra to an extent not previously observed in complexes with Ru–bpy chromophores.^{25,27,28} More generally, the *mf* vibronic sideband amplitudes observed in the 77 K emission spectra monobpy complexes range from weak and poorly resolved for low energy emitting excited states, to dominant with many resolvable features for high energy emitting states;^{25,27,28} and this work. The general pattern is that the *mf* sideband amplitudes become increasingly dominant with increasing excited-state energies in complexes with Ru–bpy chromophores.^{25–28,54,80} These sideband amplitudes are measures of the distortions of the bpy ligand (eqs 1–4 and A1–A3), and might be correlated to the variations in electronic charge on bpy in the ground and excited state.²¹ However, the computational model used here indicates that the observed pattern of sideband amplitudes arises mostly from the relative energies of the metal-centered and bpy-centered frontier orbitals, with the amount of bpy character mixed in the nominally “metal-based” SOMO increasing for high T₀ energies and decreasing for low T₀ energies. Some of the details and implications of specific observations are reviewed briefly before we develop a broader perspective on the nature of the lowest energy “MLCT” excited states in these systems.

1. Concerning the Computational Modeling of the Lowest Energy Monobpy Triplet Excited States. This modeling has reasonably approximated the different energies and band shapes found for [Ru(NH₃)₄bpy]²⁺ and [Ru(CH₃CN)₄bpy]²⁺ emission spectra (Figure 3 and Table 1). It also indicates that most of the observed contrast in band shapes arises from just the energy difference between the ground and the excited states. This model, based by varying Z_{Ru} in the DFT calculations, reproduces the observed patterns of variations in band shapes remarkably well. Furthermore, the modeling strongly implicates different origins of at least some of the *lf* (first-order spectral feature with $h\nu_{\text{vib}} \approx 300$ cm⁻¹; Figure 7) and *mf* (first-order spectral feature with $h\nu_{\text{vib}} \approx 1500$ cm⁻¹; Figure 7) vibronic components of these complexes: (a) the ratio of the calculated amplitudes of the *mf* to the *lf* features is

about 0.06 for the lowest excited-state energy considered and about 1.8 for the highest, and (b) the calculated combination bands for the *lf* and *mf* vibronic modes seem to have complementary dependencies on the excited-state energy as noted in Figures 7 and 8.

2. Estimation of the Distribution of Electronic Charge between Ru and bpy Based on the DFT Modeling. Since the differences between the ground- and the excited-state molecular structures are expected to decrease with increases in configurational mixing between them, this could be one origin of the variations in *mf* to *lf* vibronic contributions to the spectra that are noted in the preceding paragraph.^{25,27,28} This predicts that when there is appreciable ground-state/excited-state mixing the difference in nuclear coordinates and electronic charges on the bpy ligand between the lowest energy excited state and the ground state should decrease as the excited-state energy decreases.

Scarborough and Wieghardt proposed that changes in the C₁–C₁' bond length, $\Delta d(\text{C1–C1}')$, of metal–bipyridine complexes are proportional to the amount of charge on the bpy ligand,²¹ and the structural data in their report suggest that an increase of one unit of electronic charge on bpy corresponds approximately to a bond length decrease of $\Delta d(\text{C1–C1}') \approx 0.057$ Å. We used this argument in Figure 13 as a measure of

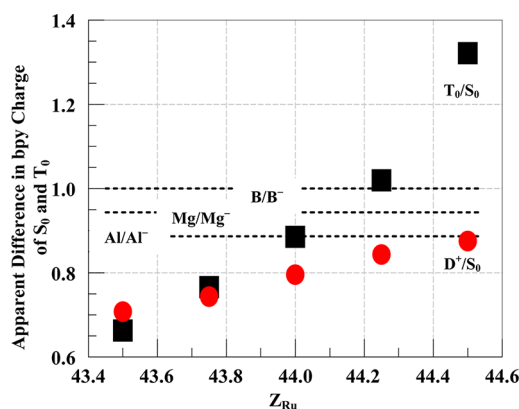


Figure 13. Calculated apparent charge difference between the S₀ and the T₀ electronic states of [Ru(NH₃)₄bpy]²⁺ as a function of Z_{Ru} (i.e., excited-state energy). On the basis of data in Table 2 with the calculated C₁–C₁' bond length difference of 0.053 Å between bpy and bpy^{•-} (abbreviated (B/B⁻) taken as equivalent to one unit of charge). Black squares are for the calculated bond length differences between the ³MLCT₀ excited state (T₀) and the ground state (S₀) of [Ru(NH₃)₄bpy]²⁺; red circles are for the calculated bond length differences between the reduced complex [Ru(NH₃)₄bpy]⁺ (D⁺) and S₀. Dashed horizontal lines are reference differences in calculated C₁–C₁' bond lengths for [Mg(NH₃)₄bpy]²⁺ and [Mg(NH₃)₄bpy^{•-}]⁺ (Mg/Mg⁻) and [Al(NH₃)₄bpy]³⁺ and [Al(NH₃)₄bpy]²⁺ (Al/Al⁺).

the difference in the charge on the bpy ligand of the [Ru(NH₃)₄bpy]²⁺ complex in its ground and lowest energy electronic excited states (S₀ and T₀, respectively) but with a 0.053 Å change in $\Delta d(\text{C1–C1}')$ for one unit change of electronic charge in order that the bond length changes calculated for the free ligand and its reduced radical anion would correspond to one unit of charge. The variations in $\Delta d(\text{C1–C1}')$ calculated for the bpy/bpy^{•-}, [Mg(NH₃)₄bpy]²⁺/[Mg(NH₃)₄bpy]⁺, and [Al(NH₃)₄bpy]²⁺/[Al(NH₃)₄bpy]⁺ pairs suggest that there is a systematic effect of about 0.002–0.004 Å of the charge on the central metal on

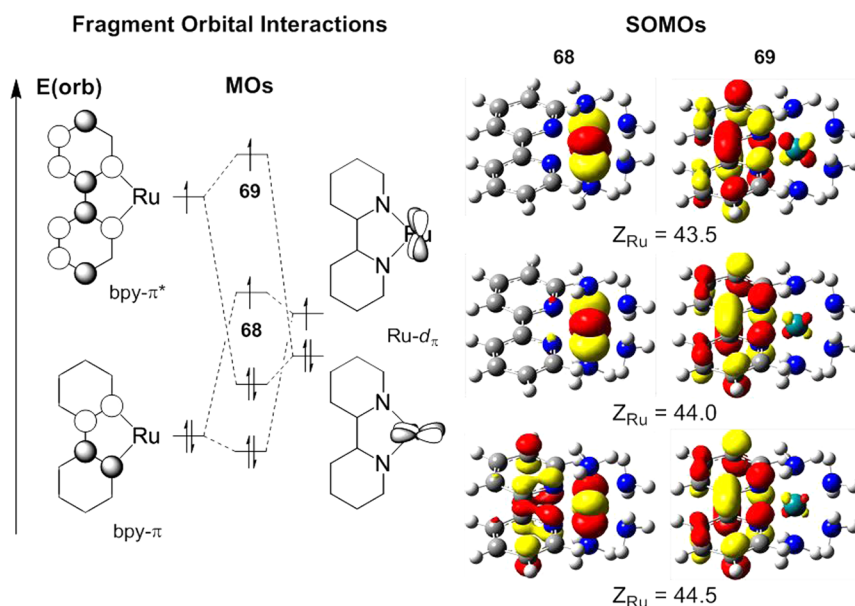


Figure 14. Fragment orbital interaction scheme (left) for the $^3\text{MLCT}$ state constructed using $\text{bpy}^{\bullet-}$ and $\text{Ru}^{\text{III}}(\text{NH}_3)_4$ fragments. Isosurface plots (0.05 au) of the SOMOs **68** and **69** (right) are plotted for three different adjustable nuclear charges at Ru (Z_{Ru}). SOMOs are arranged from bottom to top in the order of increasing $d\pi$ orbital energies.

$\Delta d(\text{C1}-\text{C1}')$ that complicates this comparison, but the overall trends are outside this range. The 0.008 Å difference in $\Delta d(\text{C1}-\text{C1}')$ for S_0 and $[\text{Ru}(\text{NH}_3)_4\text{bpy}]^+$ over the range of adjustable nuclear charges is opposite to the apparent effect of central metal charge (Al, Mg) and could be consistent with a relatively small effect of the donor/acceptor mixing discussed above. The values of $\Delta d(\text{C1}-\text{C1}')$ for S_0/T_0 are comparable to those of the $S_0/[\text{Ru}(\text{NH}_3)_4\text{bpy}^{\bullet-}]^+$ pair for the smaller values of Z_{Ru} ; thus, at sufficiently low energy the values of $\Delta d(\text{C1}-\text{C1}')$ for T_0 approach expectation for a simple charge-transfer system. However, for the highest energy $^3\text{MLCT}_0$ excited-state calculated $\Delta d(\text{C1}-\text{C1}')$ is nearly twice as large as that presumed to result from transfer of a single electron from Ru^{II} to bpy.

The band shape calculated for $Z_{\text{Ru}} = 44.5$ is very similar to those observed experimentally for the $[\text{Ru}(\text{CH}_3\text{CN})_4\text{bpy}]^{2+}$ and $[\text{Ru}([14]\text{aneS}_4)\text{bpy}]^{2+}$ complexes; the hypothesis that the vibronic sideband amplitudes are only functions of the difference in charge on the bpy ligand in the ground and excited state implies more than one unit of charge difference in these complexes. This cannot be correct, and there must be some other source for bpy ligand distortion.

3. Interpretation of the Calculated Bond Length Changes and Implications for the Variations in Vibronic Sideband Contributions. The calculated C1–C1' bond length contraction of T_0 to a value shorter than the idealized $\text{bpy}^{\bullet-}$ limit of $[\text{Ru}^{\text{III}}(\text{NH}_3)_4\text{bpy}^{\bullet-}]^{2+}$ for large Z_{Ru} values (see Figure 11) is not likely to correspond to the changes in electron density postulated²¹ to correlate with $\Delta d(\text{C1}-\text{C1}')$ since this would imply contributions of a $[\text{Ru}^{\text{IV}}(\text{NH}_3)_4\text{bpy}^{2-}]^{2+}$ species in a low-energy excited state.

In order to better understand the pattern of the C1–C1' bond lengths as a function of Z_{Ru} , we investigated the singly occupied molecular orbitals (SOMOs) of the triplet state. The SOMOs were generated through a corresponding orbital analysis⁸² that let us unambiguously determine which orbitals are singly occupied. Due to the MLCT nature of this excited state, we constructed the molecular orbitals from the diabatic

fragments $\text{bpy}^{\bullet-}$ and $\text{Ru}^{\text{III}}(\text{NH}_3)_4$ (Figure 14, left). Only four frontier orbitals are shown for clarity: the doubly occupied $\text{bpy}-\pi$, the half-occupied $\text{bpy}-\pi^*$, a correlated filled $\text{Ru}-d_{\pi}$, and the half-filled $\text{Ru}-d_{\pi^*}$ orbitals. As can be seen in the SOMO plots (Figure 14, right) for $Z_{\text{Ru}} = 44.0$, SOMOs (MO's **68** and **69**) are localized at the Ru and bpy moieties, respectively, suggesting little mixing between the fragments. Decreasing Z_{Ru} from 44.0 to 43.5 increases all orbital energies, but this impact is felt most by the orbitals centered at Ru. Thus, the energy of the $\text{Ru}-d_{\pi}$ orbitals will increase relative to the bpy-based orbitals. As a result, the bpy-centered SOMO (**69**) has slightly more Ru character (see Supporting Information Table S9 for Mulliken population analysis of these orbitals)⁵⁹ compared to $Z_{\text{Ru}} = 44.0$, while the Ru-centered SOMO (**68**) continues to have negligible ligand character. Increasing Z_{Ru} from 44.0 to 44.5 has the opposite effect; all orbitals decrease in energy with the Ru-based orbitals affected the most. This lessens the interaction between the doubly occupied $\text{Ru}-d_{\pi}$ orbital and half-occupied $\text{bpy}-\pi^*$ slightly as seen in the SOMO (**69**). Most dramatically, the Ru-centered SOMO now has considerable ligand-based character due to the orbital interaction shown in Figure 14. Similar bpy-ligand contributions are also a feature of the Ru-centered SOMO calculated for the T_0 excited state of $[\text{Ru}(\text{CH}_3\text{CN})_4\text{bpy}]^{2+}$ (see Supporting Information Figure S10)⁵⁹ but not for the S_1 excited state of $[\text{Ru}(\text{NH}_3)_4\text{bpy}]^{2+}$ (see Supporting Information Table S10 and Figure S11).⁵⁹ In an extreme limit where the $\text{Ru}-d_{\pi}$ becomes lower in energy than the $\text{bpy}-\pi$ orbital in the MLCT excited state, an electron may transfer from the doubly occupied bpy orbital to the half-filled metal (SOMO) orbital and generate a new excited state with Ru^{II} and a triplet bpy (bpy^{T}), analogous to the lowest energy luminescent excited state of $[\text{Zn}(\text{bpy})_3]^{2+}$.⁸³ It is important to note that the $\pi-\pi^*$ energy gap decreases upon bpy reduction in the MLCT state, making the $\text{bpy}-\pi$ orbital a better donor and therefore more able to donate electron density to Ru^{III} in the excited state. While we analyzed this behavior in terms of orbital delocalization, it is equivalent to view it in terms of configurational mixing between diabatic

$^3\text{MLCT}$ and the bpy-ligand $^3\pi\pi^*$ excited states. Ultimately, combination of bpy- π^* orbital occupation with its C1–C1' bonding character and deoccupation of the bpy- π orbital with some C1–C1' antibonding character leads to an overall bond contraction that is more consistent with the expected chemical behavior than is the bpy^{2-} formulation that arises if the interpretation is restricted to electron-transfer events involving only two orbitals.

In the extreme low-energy limit, when the ionization energy of Ru^{II} is equal in magnitude to the bpy affinity energy, the metal/ligand mixing will result in symmetric and antisymmetric combinations of the Ru-donor and bpy-acceptor orbitals and the symmetric combination will have a lower energy (larger ionization energy) than the remaining $d\pi$ orbitals. In this limit the $^3\text{MLCT}$ electronic configuration will correspond to promotion of an electron from these nonmixed $d\pi$ orbitals to the antisymmetric combination of the D and A orbitals. Thus, there will be a larger change in electronic occupation of metal-centered orbitals than bpy orbitals and correspondingly larger distortions in the metal–ligand modes and relatively smaller distortions in bpy modes.

CONCLUSIONS

We computationally modeled the $^3\text{MLCT}$ excited-state distortions and emission band shapes of monobpy Ru^{II} complexes. These complexes have been experimentally observed to have a wide range of MLCT excited-state energies and very large $E^{0,0}$ -dependent variations in the vibronic contributions to their emission band shapes. The TD-DFT modeling has shown that (1) the excited-state distortions of these complexes and the vibronic sideband contributions to their emission spectra are expected to vary systematically with the $E^{0,0}$ even when there is no variation of the ancillary ligands and (2) the $E^{0,0}$ dependencies of the T_0 distortion can be ascribed largely to differences in the amount of mixing between ground-state-Ru($d\pi$) and bpy(π^*) orbitals and/or between the excited-state Ru($d\pi$) and bpy(π) orbitals, with the former more important for the lowest and the latter for the highest T_0 energies. Thus, computational modeling indicates that tuning the ionization energy of the Ru^{II} center by changing the ancillary ligands has the effect of moving the Ru($d\pi$) orbital system across the bpy(π/π^*) orbital energy range as illustrated in Figure 15. However, the mixings of electronic states must involve different orbitals at the energy extremes since the ground-state/excited-state mixing must be predominantly within the singlet spin manifold while the $d\pi/\pi\pi^*$ mixing is between $^3\text{MLCT}$ and $^3\pi\pi^*$ excited states. The ancillary ligands which are used to experimentally modify the Ru($d\pi$) orbital ionization energies (and Z_{eff}) for the complexes that span much of this energy range can also contribute significantly to the experimentally observed vibronic sidebands; this is especially the case for some of the anionic ligands used to obtain low-energy MLCT excited states.⁵⁴

TD-DFT computational modeling of the $^3\text{MLCT}$ excited states has reproduced many of the experimental details of the monobpy complex emission spectra, and it has provided insight into the origins of the dramatic variations in band shapes found for these complexes. This approach provides the best model of the triplet Ru–bpy MLCT excited states at this time. It indicates that there are differences in the vibronic distortions in the $^1\text{MLCT}$ (S_1) and $^3\text{MLCT}$ (T_0) excited states of $[\text{Ru}(\text{NH}_3)_4\text{bpy}]^{2+}$ even though their orbital occupations are the same in the diabatic limit. The very similar but small vertical

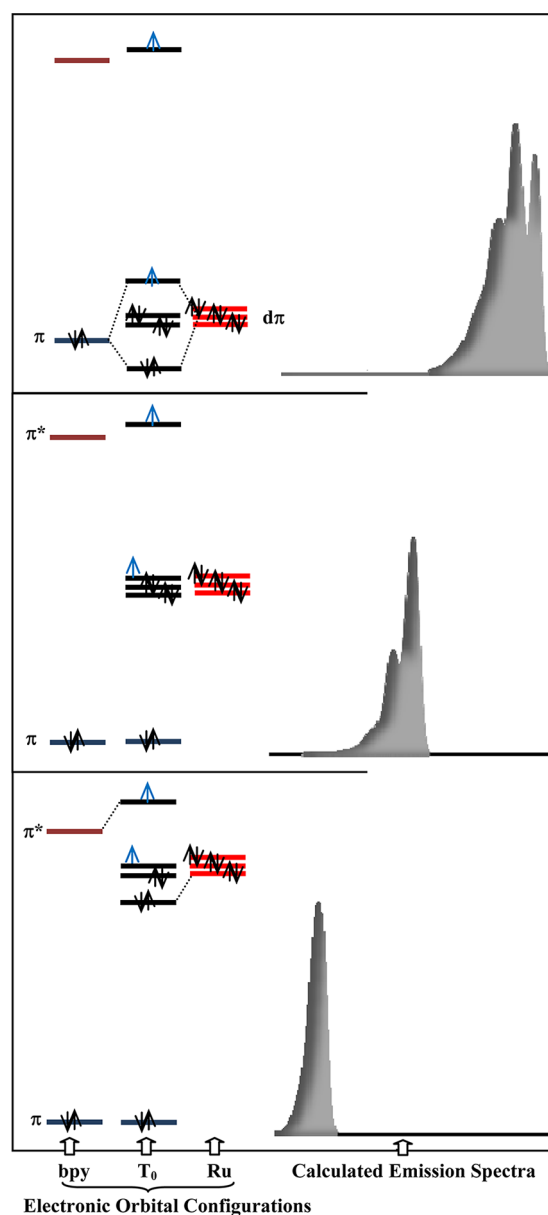


Figure 15. Qualitative illustration of the variations in orbital compositions for the T_0 electronic state and calculated emission band shape of Ru–bpy complexes with the metal ionization energy. For purposes of this illustration, the energies of the bpy ligand-centered π -bonding and π^* -antibonding orbitals (left side; bpy) are held constant and the metal-centered $d\pi$ orbital energies (middle; Ru) are varied. Interactions between these two orbital sets are determined only by their relative energies. Blue arrows indicate the singly occupied T_0 orbitals, and the energy difference between these orbitals qualitatively correlates with the T_0 energy. In the lower panel it is assumed that one Ru($d\pi$) orbital is mixed with the bpy(π^*) orbital to form ground-state bonding and antibonding orbitals of mixed metal/ligand character. In the upper panel it is assumed that a bpy(π) orbital mixes with a Ru($d\pi$) orbital to form excited-state bonding and antibonding orbitals of mixed metal/ligand character.

reorganizational energies calculated for $S_0 \rightarrow S_1$ and $T_0 \rightarrow S_0$ (1350 cm^{-1}) combined with the dissimilarity of the distribution of mf and lf distortions in these excited states implies that there is more bpy ligand distortion in T_0 than in S_1 . This difference may arise in part from more configurational mixing between the MLCT and the $\pi\pi^*$ excited states in the former than in the

latter. The difference in the energies of the S_1 and T_0 PE minima (ΔE_{ST}) calculated for these excited states is similar in magnitude to their reorganizational energies.

While this study has modeled the energy-dependent structural changes in MLCT excited states with reference to Ru–bpy complexes, the general patterns of the structural changes as a function of the metal donor energy relative to the frontier orbitals of the aromatic acceptor ligand should be a general feature of MLCT excited states.

APPENDIX I. FRANCK–CONDON FACTORS

While the excited-state distortions of the systems considered here are in more than 10 vibrational modes, the basic definitions of parameters and properties of vibronic sidebands of the more complicated systems are illustrated in the limit for which the excited-state distortions are in a single vibrational mode. In this limit the emission envelopes observed for a simple transition between a “pure” MLCT excited state and the ground state can be expressed as^{20,84–89}

$$I_f = B\nu_e^3 M_{eg}^2 F(\nu_m) \quad (A1)$$

$$F(\nu_m) = \sum_{j=0}^{\infty} F_j \exp\left(-\frac{(h\nu_m - jh\nu_{vib} - h\nu_{0'0} + \lambda_s)^2}{4\lambda_s k_B T}\right) \quad (A2)$$

$$F_j = \frac{e^{-S} S^j}{j!} \text{ and } S = \frac{\lambda_{vib}}{h\nu_{vib}} \quad (A3)$$

where M_{eg} is the transition dipole, $B = (64\pi^4)/3hc^3 \ln 10 \eta^3 / ((4\pi\lambda_s k_B T)^{1/2})$, η is the index of refraction, k_B is Boltzmann's constant, $h\nu_{vib} \gg k_B T$, λ_s is the combination of the reorganizational energies of the solvent and other displacement modes with $h\nu_{vib} < 4k_B T$, λ_{vib} is the reorganizational energy of a displacement mode with $h\nu_{vib} > 4k_B T$, and c is the speed of light. For D/A complexes, the transition dipole may be represented by^{90–92}

$$M_{eg} \approx \frac{H_{eg} \Delta\mu_{eg}}{h\nu_e} \quad (A4)$$

where H_{eg} is the excited-state–ground-state mixing matrix element and $\Delta\mu_{eg}$ is the difference between the ground- and the excited-state molecular dipole moments.^{20,89} The actual TD-DFT calculations were performed with the full formalism outlined by Barone and co-workers.^{50–53,76}

ASSOCIATED CONTENT

Supporting Information

Synthetic details and ^1H NMR spectra; table of Cartesian coordinates for all optimized species; table of solution-phase free energies (au) for optimized species; figure comparing [Ru(X-acac)₂bpy] emission spectra; skeletal structures of some ligands; normal mode displacements for active modes of S_0 ; comparison of S_1 and T_0 reorganizational energies; frequencies calculated for T_0 and S_1 distortion modes of [Ru(NH₃)₄bpy]²⁺ and those inferred from the rR spectrum; Mulliken spin densities for the triplet SOMOs; figure for SOMOs of [Ru(bpy)(CH₃CN)₄]²⁺ S_1 ; figure of donor and acceptor natural transition orbitals for the S_1 state of [Ru(bpy)(NH₃)₄]²⁺; complete citation for the Gaussian program. This material is available free of charge via the Internet at <http://pubs.acs.org>.

AUTHOR INFORMATION

Corresponding Author

*E-mail: jfe@chem.wayne.edu (F.F.E.); hbs@chem.wayne.edu (H.B.S.).

Notes

The authors declare no competing financial interest.

ACKNOWLEDGMENTS

This work was funded in part by the Division of Chemical Sciences, Geosciences, and Biosciences, Office of Basic Energy Sciences of the U.S. Department of Energy (J.F.E. and H.B.S.) through Grants DE-FG02-88ER13944 and DE-FG02-09ER16120, Office of the Vice President for Research of Wayne State University, and National Science Council of R.O.C (Y.-J.C.) through Grants NSC-95-2113-M-030-003 and NSC-96-2113-M-030-006-MY2.

REFERENCES

- (1) Crosby, G. A. *Acc. Chem. Res.* **1975**, *8*, 231.
- (2) Juris, A.; Balzani, V.; Barigelletti, F.; Compagna, S.; Belser, P. I.; von Zelewsky, A. *Coord. Chem. Rev.* **1988**, *84*, 85.
- (3) Kalyanasundaram, K. *Photochemistry of Polypyridine and Porphyrin Complexes*; Academic Press: New York, 1992.
- (4) In *Electron Transfer in Chemistry*; Balzani, V., Ed.; Wiley-VCH: Weinheim, Germany, 2001; Vols. 1–5.
- (5) Balzani, V.; Credi, A.; Venturi, M. In *Stimulating Concepts in Chemistry*; Voegtle, F., Stoddart, J. F., Shibasaki, M., Eds.; Wiley-VCH Verlag GmbH & Co. KGaA: Weinheim, Germany, 2000; p 255.
- (6) Balzani, V. *Supramolecular Photochemistry*; Reidel: Dordrecht, Germany, 1987.
- (7) Barbara, P. F.; Meyer, T. J.; Ratner, M. *J. Phys. Chem.* **1996**, *100*, 13148.
- (8) Graetzel, M.; Moser, J.-E. In *Electron Transfer in Chemistry*; Balzani, V., Ed.; Wiley-VCH: Weinheim, 2001; Vol. 5, p 589.
- (9) Graetzel, M. *Inorg. Chem.* **2005**, *44*, 6841.
- (10) Campagna, S.; Serroni, S.; Puntoriero, F.; Di Pietro, C.; Ricevuto, V. In *Electron Transfer in Chemistry*; Balzani, V., Ed.; Wiley-VCH: Weinheim, 2001; Vol. 5, p 186.
- (11) Scandola, F.; Chiorboli, C.; Indelli, M. T.; Rampi, M. A. In *Electron Transfer in Chemistry*; Balzani, V., Ed.; Wiley-VCH: Weinheim, 2001; Vol. 3, p 337.
- (12) Vaidyalingham, A. S.; Coutant, M. A.; Dutta, P. K. In *Electron Transfer in Chemistry*; Balzani, V., Ed.; Wiley-VCH: Weinheim, 2001; Vol. 4, p 412.
- (13) Venturi, M.; Credi, A.; Balzani, V. In *Electron Transfer in Chemistry*; Balzani, V., Ed.; Wiley-VCH: Weinheim, 2001; Vol. 3, p 501.
- (14) Hahn, U.; Gorke, M.; Vogtle, F.; Vicinelli, V.; Ceroni, P.; Maestri, M.; Balzani, V. *Angew. Chem., Int. Ed.* **2002**, *41*, 3595.
- (15) Serroni, S.; Campagna, S.; Puntoriero, F.; Juris, A.; Denti, G.; Balzani, V.; Venturi, D.; Janzen, D.; Mann, K. R. *Inorg. Synth.* **2002**, *33*, 10.
- (16) Marcus, R. A. *J. Chem. Phys.* **1965**, *43*, 670.
- (17) Newton, M. D.; Sutin, N. *Annu. Rev. Phys. Chem.* **1984**, *35*, 437.
- (18) Endicott, J. F. In *Electron Transfer in Chemistry*; Balzani, V., Ed.; Wiley-VCH: New York, 2001; Vol. 1, p 238.
- (19) Endicott, J. F. In *Comprehensive Coordination Chemistry II*, 2nd ed.; McCleverty, J., Meyer, T. J., Eds.; Pergamon: Oxford, U.K., 2003; Vol. 7, p 657.
- (20) Gould, I. R.; Noukakis, D.; Gomez-Jahn, L.; Young, R. H.; Goodman, J. L.; Farid, S. *Chem. Phys.* **1993**, *176*, 439.
- (21) Scarborough, C. C.; Wieghardt, K. *Inorg. Chem.* **2011**, *50*, 9773.
- (22) Hupp, J. T.; Williams, R. T. *Acc. Chem. Res.* **2001**, *34*, 808.
- (23) Maruszewski, K.; Bajdor, K.; Strommen, D. P.; Kincaid, J. R. *J. Phys. Chem.* **1995**, *99*, 6286.
- (24) Thompson, D. G.; Schoonover, J. R.; Timpson, C. J.; Meyer, T. J. *J. Phys. Chem. A* **2003**, *107*, 10250.

- (25) Chen, Y.-J.; Xie, P.; Heeg, M. J.; Endicott, J. F. *Inorg. Chem.* **2006**, *45*, 6282.
- (26) Odongo, O. S.; Endicott, J. F. *Inorg. Chem.* **2009**, *48*, 2818.
- (27) Odongo, O. S.; Heeg, M. J.; Chen, J. Y.; Xie, P.; Endicott, J. F. *Inorg. Chem.* **2008**, *47*, 7493.
- (28) Xie, P.; Chen, Y.-J.; Uddin, M. J.; Endicott, J. F. *J. Phys. Chem. A* **2005**, *109*, 4671.
- (29) Caspar, J. V.; Kober, E. M.; Sullivan, B. P.; Meyer, T. J. *J. Am. Chem. Soc.* **1982**, *104*, 630.
- (30) Kober, E. M.; Casper, J. V.; Lumpkin, R. S.; Meyer, T. J. *J. Phys. Chem.* **1986**, *90*, 3722.
- (31) Litke, S. V.; Ershov, A. Y.; Meyer, T. J. *J. Phys. Chem. A* **2011**, *115*, 14235.
- (32) Krishnan, R.; Binkley, J. S.; Seeger, R.; Pople, J. A. *J. Chem. Phys.* **1980**, *72*, 650.
- (33) Perdew, J. P. *Phys. Rev. B* **1986**, *33*, 8822.
- (34) Becke, A. D. *J. Chem. Phys.* **1993**, *98*, 5648.
- (35) Perdew, J. P.; Burke, K.; Wang, Y. *Phys. Rev.* **1996**, *54*, 16533.
- (36) Ciofini, I.; Daul, C. A.; Adamo, C. *J. Phys. Chem. A* **2003**, *107*, 11182.
- (37) Alary, F.; Heully, J.-L.; Bijere, L.; Vicendo, P. *Inorg. Chem.* **2007**, *46*, 3154.
- (38) Abrahamsson, M.; Lundqvist, M. J.; Wolpher, H.; Johansson, O.; Eriksson, L.; Bergquist, J.; Rasmussen, T.; Becker, H.-C.; Hammarstroem, L.; Norrby, P.-O.; et al. *Inorg. Chem.* **2008**, *47*, 3540.
- (39) Alary, F.; Boggio-Pasqua, M.; Heully, J.-L.; Marsden, C. J.; Vicendo, P. *Inorg. Chem.* **2008**, *47*, 5259.
- (40) Salassa, L.; Garino, C.; Salassa, G.; Gobetto, R.; Nervi, C. *J. Am. Chem. Soc.* **2008**, *130*, 9590.
- (41) Borg, O. A.; Godinho, S. S. M. C.; Lundqvist, M. J.; Lunell, S.; Persson, P. *J. Phys. Chem. A* **2008**, *112*, 4470.
- (42) Salassa, L.; Garino, C.; Salassa, G.; Nervi, C.; Gobetto, R.; Lamberti, C.; Gianolio, D.; Bizzarri, R.; Sadler, P. J. *Inorg. Chem.* **2009**, *48*, 1469.
- (43) Jakubikova, E.; Chen, W.; Dattelbaum, D. M.; Rein, F. N.; Rocha, R. C.; Martin, R. L.; Batista, E. R. *Inorg. Chem.* **2009**, *48*, 10720.
- (44) Heully, J.-L.; Alary, F.; Boggio-Pasqua, M. *J. Chem. Phys.* **2009**, *131*, 184308.
- (45) Dixon, I. M.; Alary, F.; Heully, J.-L. *Dalton Trans.* **2010**, *39*, 10959.
- (46) Jakubikova, E.; Martin, R. L.; Batista, E. R. *Inorg. Chem.* **2010**, *49*, 2975.
- (47) Sun, Y.; El Ojaimi, M.; Hammit, R.; Thummel, R. P.; Turro, C. *J. Phys. Chem. B* **2010**, 14664.
- (48) Gottle, A. J.; Dixon, I. M.; Alary, F.; Heully, J., -L.; Boggio-Pasqua, M. *J. Am. Chem. Soc.* **2011**, *133*, 9172.
- (49) Lebon, E.; Bastin, S.; Sutra, P.; Vendier, L.; Piau, R. E.; Dixon, I. M.; Boggio-Pasqua, M.; Alary, F.; Heully, J.-L.; Igau, A.; et al. *Chem. Comm* **2012**, *48*, 741.
- (50) Oesterman, T.; Abrahamsson, M.; Becker, H.-C.; Hammarstroem, L.; Persson, P. *J. Phys. Chem. A* **2012**, 1041.
- (51) Santoro, F.; Improta, R.; Lami, A.; Bloino, J.; Barone, V. *J. Chem. Phys.* **2007**, *126*, 084509.
- (52) Santoro, F.; Improta, R.; Lami, A.; Bloino, J.; Barone, V. *J. Chem. Phys.* **2007**, *126*, 169903.
- (53) Santoro, F.; Lami, A.; Improta, R.; Barone, V. *J. Chem. Phys.* **2007**, *126*, 184102.
- (54) Allard, M. M.; Odongo, O. S.; Lee, M. M.; Chen, Y.-J.; Endicott, J. F.; Schlegel, H. B. *Inorg. Chem.* **2010**, *49*, 6840.
- (55) Dwyer, F. P.; Goodwin, H. A.; Gyrfas, E. C. *Aust. J. Chem.* **1963**, *16*, 544.
- (56) Petroni, A.; Slep, L. D.; Etchenique, R. *Inorg. Chem.* **2008**, *47*, 951.
- (57) Adams, H.; Amado, A. M.; Felix, V.; Mann, B. E.; Antelo-Martinez, J.; Newell, M.; Ribeiro-Claro, P. J. A.; Spey, S. E.; Thomas, J. A. *Chem.—Eur. J.* **2005**, *11*, 2031.
- (58) Eskelinen, E.; Da Costa, P.; Haukka, M. *J. Electroanal. Chem.* **2005**, *579*, 257.
- (59) Supporting Information.
- (60) Rhodes, T. A.; Farid, S.; Goodman, J. L.; Gould, I. R.; Young, R. H. *J. Am. Chem. Soc.* **1999**, *121*, 5340.
- (61) Chen, Y.-J.; Xie, P.; Endicott, J. F. *J. Phys. Chem. A* **2004**, *108*, 5041.
- (62) Parr, R. G.; Yang, W. *Density-functional theory of atoms and molecules*; Oxford University Press: New York, 1989.
- (63) Frisch, M. J.; Trucks, G. W.; Schlegel, H. B.; et al. *Gaussian Development Version*, Revision H.09+; Gaussian: Wallingford, CT, 2010. Complete citation in Supporting Information S12.
- (64) Tsai, C.-N.; Allard, M. M.; Lord, R. L.; Luo, D.-W.; Chen, Y.-J.; Schlegel, H. B.; Endicott, J. F. *Inorg. Chem.* **2011**, *50*, 8274.
- (65) Andrae, D.; Haussermann, U.; Dolg, M.; Stoll, H.; Preuss, H. *Theor. Chim. Acta* **1990**, *77*, 123.
- (66) Dunning, T. H., Jr.; Hay, P. J. In *Modern Theoretical Chemistry*; Schaefer, H. F., III, Ed.; Plenum: New York, 1976; Vol. 3, p 1.
- (67) Igelmann, G.; Stoll, H.; Preuss, H. *Mol. Phys.* **1988**, *65*, 1321.
- (68) Schlegel, H. B.; McDouall, J. J. In *Computational Advances in Organic Chemistry*; Ögretir, C., Csizmadia, I. G., Eds.; Kluwer Academic: Amsterdam, The Netherlands, 1991.
- (69) Bauernschmitt, R.; Ahlrichs, R. *J. Chem. Phys.* **1996**, *104*, 9047.
- (70) Schlegel, H. B. *J. Comput. Chem.* **1982**, *3*, 214.
- (71) Miertuš, S.; Scrocco, E.; Tomasi, J. *Chem. Phys.* **1981**, *55*, 117.
- (72) Tomasi, J.; Mennucci, B.; Cammi, R. *Chem. Rev.* **2005**, *105*, 2999.
- (73) Scalmani, G.; Frisch, M. J.; Mennucci, B.; Tomasi, J.; Cammi, R.; Barone, V. *J. Chem. Phys.* **2006**, 124.
- (74) Scalmani, G.; Frisch, M. J. *J. Chem. Phys.* **2010**, 132.
- (75) Pennington, R.; Keith, T.; Millam, J. M.; GaussView V. 5.0, Semichem, Inc.: Shawnee Mission, KS, 2009.
- (76) Santoro, F.; Lami, A.; Improta, R.; Bloino, J.; Barone, V. *J. Chem. Phys.* **2008**, *128*, 224311.
- (77) Bard, A. J.; Faulkner, L. R. *Electrochemical Methods*; Wiley: New York, 1980.
- (78) Birks, J. B. *Photophysics of Aromatic Molecules*; Wiley-Interscience: New York, 1970.
- (79) Mulliken, R. S.; Person, W. B. *Molecular Complexes*; Wiley-Interscience: New York, 1967.
- (80) Chen, Y.-J.; Endicott, J. F.; Swayambunathan, V. *Chem. Phys.* **2006**, *326*, 79.
- (81) Shin, Y. K.; Szalda, D. J.; Brunschwig, B. S.; Creutz, C.; Sutin, N. *Inorg. Chem.* **1997**, *36*, 3190.
- (82) Neese, F. *J. Phys. Chem. Solids* **2004**, *65*, 781.
- (83) Nozaki, K.; Takamori, K.; Nakatsugawa, Y.; Ohno, T. *Inorg. Chem.* **2006**, *45*, 6161.
- (84) Englman, R.; Jortner, J. *Mol. Phys.* **1970**, *18*, 145.
- (85) Ulstrup, J.; Jortner, J. *J. Chem. Phys.* **1975**, *63*, 4338.
- (86) Myers, A. B. *Chem. Phys.* **1994**, *180*, 215.
- (87) Myers, A. B. *Acc. Chem. Res.* **1997**, *30*, 519.
- (88) Myers, A. B. *Chem. Rev.* **1996**, *96*, 911.
- (89) Mukherjee, T.; Ito, N.; Gould, I. R. *J. Phys. Chem. A* **2011**, *115*, 1837.
- (90) Mulliken, R. S. *J. Am. Chem. Soc.* **1952**, *74*, 811.
- (91) Hush, N. S. *Prog. Inorg. Chem.* **1967**, *8*, 391.
- (92) Hush, N. S. *Electrochim. Acta* **1968**, *13*, 1005.